Origin of intrinsic irregular firing in cortical interneurons

Klaus M. Stiefel[a,b,c,1], Bernhard Englitz[a,b,c,2], and Terrence J. Sejnowski[a,b,c,d,3]

[a]Computational Neurobiology Laboratory and [b]Howard Hughes Medical Institute, [c]Salk Institute for Biological Studies, La Jolla, CA 92037; and [d]Division of Biological Sciences, University of California at San Diego, La Jolla, CA 92093

Contributed by Terrence J. Sejnowski, March 22, 2013 (sent for review July 29, 2012)

Cortical spike trains are highly irregular both during ongoing, spontaneous activity and when driven at high firing rates. There is uncertainty about the source of this irregularity, ranging from intrinsic noise sources in neurons to collective effects in large-scale cortical networks. Cortical interneurons display highly irregular spike times (coefficient of variation of the interspike intervals >1) in response to dc-current injection in vitro. This is in marked contrast to cortical pyramidal cells, which spike highly irregularly in vivo, but regularly in vitro. We show with in vitro recordings and computational models that this is due to the fast activation kinetics of interneuronal K^+ currents. This explanation holds over a wide parameter range and with Gaussian white, power-law, and Ornstein–Uhlenbeck noise. The intrinsically irregular spiking of interneurons could contribute to the irregularity of the cortical network.

inhibitory interneuron | bistability | neural noise | fluctuations | cortex

When spike trains of cortical pyramidal neurons are recorded in vivo from the cortices of awake or sleeping cats (1–3) or awake monkeys (4), the interspike intervals (ISIs) are highly variable, with coefficients of variation (CV_{ISI} = ISI SD/ISI mean) >1. However, when the main cortical excitatory (pyramidal) neurons are depolarized in vitro by injection of constant current to above firing threshold, their spike trains are substantially more regular (CV_{ISI} <0.5). The irregularity of pyramidal neuron firing in vivo arises from the intense, ongoing, temporally correlated synaptic activity that bombards cortical neurons (1, 2, 5–7). The lower in vitro irregularity can be raised to in vivo levels by using fluctuating current injection (8), hyperosmolar solution (9), and a neuromodulatory mixture (10, 11).

Computational models of irregular neuronal firing typically include network synaptic activity represented by stochastic aggregate processes. Fluctuating inputs have been represented by Brownian motion (12) or an Ornstein–Uhlenbeck process (8) in both single- and multicompartmental neuronal models (5). These are externally induced fluctuations and do not mechanistically explain the variety of irregular discharge patterns observed in cortical interneurons. In this study we combined in vitro recordings and computational models of cortical interneurons to show how neuronal conductances interact with the stochastic input to produce the variety of observed neuronal phenotypes.

Results

Recordings from Cortical Inhibitory Interneurons. Cortical GABAergic interneurons have a range of functions including the gating (13) and entrainment (14) of neuronal firing, dendritic integration (15), synaptic plasticity (16), and the generation of network oscillations (10, 11). There are several morphologically and physiologically distinct classes of interneurons (17).

In contrast to pyramidal neurons, a constant current injected into mouse visual cortex layer 2/3 interneurons in vitro frequently produced a spike train with a CV_{ISI} that substantially exceeds 1, often producing highly irregular sequences of burst. This observation is in accord with earlier descriptions of spike trains of these interneurons and used as a criterion in interneuron classifications (17, 18). The irregular spike trains were observed even under blockade of glutamatergic and GABAergic synaptic transmission and thus must be a consequence of an intrinsic process. Their intrinsically irregular spike trains hence make interneurons plausible candidates for the origin of cortical spiking irregularity.

We made multiple, long recordings from 14 interneurons and classified them according to their firing patterns as described in Markram et al. (17). In short, when depolarized by a step pulse just above rheobase, the firing patterns potentially display accommodation (successive lengthening of ISIs) and irregular clustering of spikes to different degrees (irregular spiking to stuttering). The accommodating and nonaccommodating neurons are further subdivided into classic, bursting, and delayed firing neurons (c, b, and d).

Of the neurons we recorded from, four were stuttering neurons (ST; Fig. 1*A*), four were irregular spiking (IS; Fig. 1*B*), three were nonaccommodating (NA; one each of the c-, b- and d-NA type, Fig. 1*C*), and three were accommodating (AC; all c-AC, Fig. 1*D*). For comparison purposes, we also recorded from two pyramidal neurons (Fig. 1*E*). As expected, the pyramidal cells emitted regular spike trains in response to current-step injection, as did the AC and NA interneurons. In contrast, the ST and IS interneurons displayed highly irregular spike trains in response to current-step injection, some even at high discharge rates (CV_{ISI} = 1.21 at 28 Hz).

The spike trains of ST and IS interneurons firing at low frequencies consisted of individual spikes spaced at irregular intervals. Bursts occurred at higher frequencies, with the spikes within each burst separated by afterhyperpolarization (AHP) (Fig. 1*F*). There was no voltage envelope below the bursts as in thalamic relay neurons (19). At even higher frequencies these bursts fused, leading to continuous spiking and a drop in CV_{ISI} below 0.5 in five of eight cells tested above a cell-specific frequency. Thus, we observed an inverse dependence of the CV_{ISI} on the firing frequency in these cells.

In a related study, we demonstrated, using nonlinear time-series analysis, that the interspike intervals of ST and IS interneuron spike trains were purely stochastic and showed no detectable signs of higher-order determinism or chaos (20). We therefore searched for alternative, stochastic mechanisms that could generate the irregular spike trains.

Subthreshold voltage fluctuations occur in pyramidal cells and interneurons and are voltage-dependent (Fig. 2). The most likely source of membrane potential noise in pharmacologically isolated neurons in slices is fluctuating ion channel gating, which is voltage-dependent (21). Although the amplitude of the noise in the membrane potential is predicted to be small, the extrapolated

Author contributions: K.M.S., B.E., and T.J.S. designed research; K.M.S. and B.E. performed research; K.M.S., B.E., and T.J.S. analyzed data; and K.M.S., B.E., and T.J.S. wrote the paper.

The authors declare no conflict of interest.

Freely available online through the PNAS open access option.

[1]Present address: Bioelectronics and Neuroscience, MARCS Institute, University of Western Sydney, Penrith, NSW 2751, Australia.

[2]Present address: Institute for Systems Research, University of Maryland, College Park, MD 20742.

[3]To whom correspondence should be addressed. E-mail: terry@salk.edu.

This article contains supporting information online at www.pnas.org/lookup/suppl/doi:10.1073/pnas.1305219110/-/DCSupplemental.

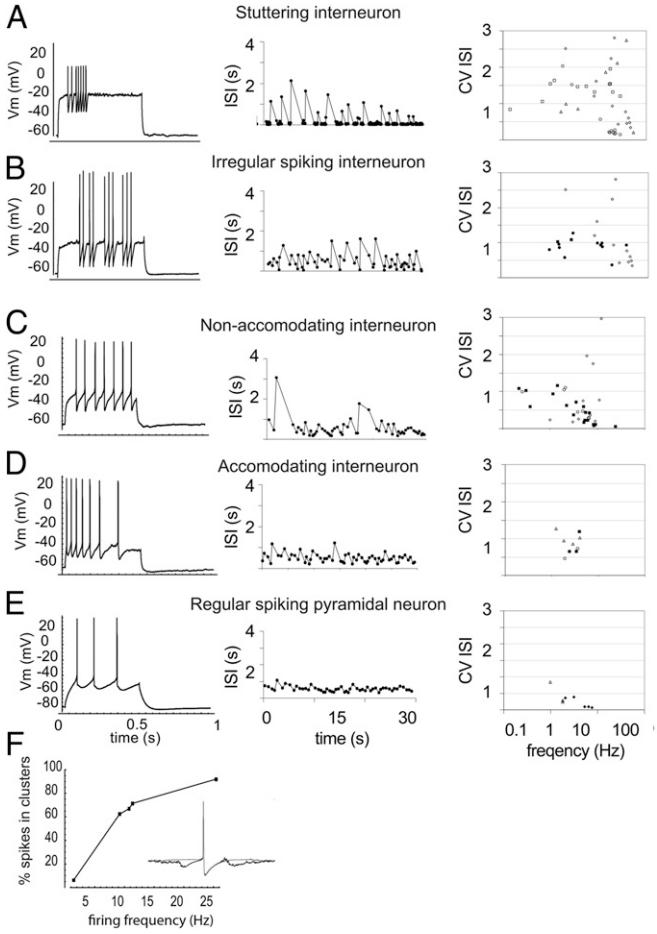

Fig. 1. Regular and irregular action potential firing in cortical pyramidal cells and interneurons. Firing pattern in response to a depolarizing current pulse (*Left*), ISIs during a 30-second spike train in response to dc depolarization (*Center*) and the CV of the ISIs as a function of the firing frequency (*Right*). Data from (*A*) ST, (*B*) IS, (*C*) NAC, and (*D*) AC interneurons and (*E*) regular firing pyramidal cells. Resting potential (mV) and input resistance (MΩ) in these cell types were as follow: ST, −67 ± 6 mV/218 ± 154 MΩ; IS, −63 ± 11 mV/376 ± 171 MΩ; AC, −72 ± 13 mV/189 ± 36 MΩ; NAC, −79 ± 7 mV/165 ± 43 MΩ; and Py, −72 ± 13 mV/189 ± 35 MΩ. (*F*) Percentage of spikes in clusters as a function of the firing frequency in a ST interneuron. (*Inset*) Averaged spike waveforms of spikes within a cluster (solid black line) and in isolation (gray line).

noise at firing threshold is actually larger in pyramidal neurons (Table 1), which have the most regular interspike intervals. Different amplitudes of voltage noise could therefore not explain the differences in the CV_{ISI}. The difference between pyramidal neurons and interneurons must thus be found in their susceptibility to transform these subthreshold fluctuations into spike-time variability.

Biophysical Simulations of Pyramidal Neurons and Interneurons. One obvious difference in the spike waveforms of interneurons and pyramidal cells is the duration of the AHP (Fig.1), which is much shorter in interneurons than in pyramidal cells. This is caused by the faster activation time constants (τ_s) of the K^+ currents mediating the AHP. In pyramidal cells, the currents mediating the AHP are I_{AHP}, I_{AHPs}, and I_M. These currents have τ time constants ranging from 70 ms to 200 ms (21, 22). In interneurons, the AHP is mediated by I_{KDR}-type K^+ currents and I_D, with time constants ranging from 5 ms to 20 ms. We explored the role of this difference in a single-compartmental neuronal model, which is an expansion of the classic Hodgkin–Huxley equations (with parameters reproducing cortical spiking) by one conductance, a K^+ current involved in the AHP (*Methods*). In this case, g_{KS} does not represent a specific current, but serves as an abstraction for the sum of all K^+ currents involved in the AHP.

We varied the time constant of this K^+ current from the interneuronal range (τ_s ~6 ms) to the pyramidal range (τ_s ~200 ms) with all of the other conductances remaining the same. The kinetics of the K^+ conductance used in the simulations is given in *Methods*. A single K^+ conductance gating time constant τ_m was varied over the range found in the AHPs of interneurons (fast τ_s) and pyramidal cells (slow τ_s). We found that faster τ_s produced higher output spike variability (Fig. 3). This effect was also not dependent on the different firing rates between models with a fast and a slow τ_s (Fig. 3*E*).

To further investigate the connection between τ_s and spike-time irregularity, we observed the dynamics of spiking neurons on a phase plane (Fig. 3, *Center*). The axes of the phase plane were the activation variable (s) of the K^+ conductance mediating the AHP and the voltage (V_m). The state of the neuron at any point in time corresponds to a point on a phase plane. The complete phase plane for this five-dimensional model would be a five-dimensional hyperplane. However, we restricted the analysis to V_m and s, because these are the most relevant state variables for the question of spiking irregularity. During a periodic behavior such as spiking, the state of the neuron moves on the phase plane around a closed orbit called a "limit cycle."

In the absence of noise, when τ_s was slow (200 ms, pyramidal neuron), the range over which s changed was small (±0.006, 0.036–0.042), leading to limit cycle compressed in the s-axis. In contrast, when τ_s was fast (6 ms, interneuron), s ranged over a wider extent (±0.159, 0.024–0.183) during the limit cycle. In both cases, the trajectory on the phase plane followed a single limit cycle, corresponding to the spike.

In simulations with slow τ_s (200 ms, pyramidal neuron) the introduction of noise led to jitter in the path around the limit cycle, corresponding to spike-time jitter. However, the phase plane trajectory still followed a single limit cycle. In contrast, with fast τ_s (6 ms, interneuron) the trajectory on the phase plane

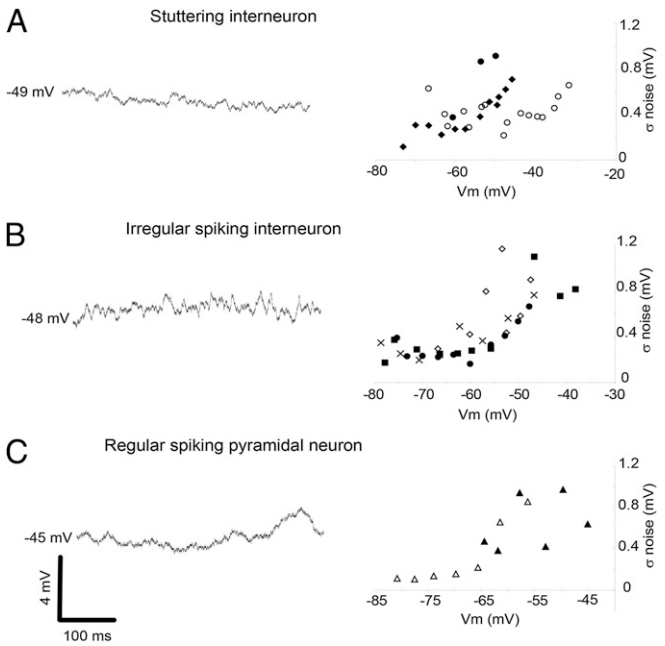

Fig. 2. Subthreshold noise in cortical pyramids and interneurons. Subthreshold noise amplitude as a function of voltage (*Right*) and example voltage traces (at the indicated dc voltage, *Right*) of ST (*A*) and IS (*B*) interneurons and pyramids (*C*). Different symbols correspond to individual neurons.

Table 1. Voltage noise in cortical neurons

Neuron type	σ/V_m, mV/mV	Threshold, mV	σ at threshold, mV
Pyramidal neuron	0.02245	−38	1.08
IS Interneuron	0.01742	−39.5	0.80
ST Interneuron	0.02403	−33.3	1.04

The noise amplitude as a function of the membrane potential, the action potential firing threshold and the extrapolated noise amplitude at threshold are indicated.

either followed the limit cycle corresponding to the spike or a smaller cycle, corresponding to a subthreshold oscillation (such as those described in ref. 23). When the state of the neuron passed a switching region just below firing threshold (depicted by a die in Fig. 3*A*, *Center*) it stochastically decided between the stable limit cycle (the spike) or a trajectory around a stable fixed point (the resting potential) of a Hopf–Andronov bifurcation (24, 25). Larger and faster upward fluctuations in the switching region would propel the behavior of the neuron from subthreshold oscillating to spiking, but smaller and slower fluctuations favored the fixed point. Once the neuron is locked in either the spiking or the subthreshold-oscillating behavior, it remains there in the absence of sufficiently large fluctuations occurring in the switching region. This explains the temporal clustering of spikes seen in IS and ST interneurons.

Hence, there was a qualitative change of spiking dynamics, caused by an interaction between fast K^+ conductance dynamics and the introduction of noise. This high sensitivity to noise is also indicative of the vicinity of the system to a bifurcation (26).

Bifurcation Analysis. The noise-induced transitions we observed were dependent on the bistability between spiking and subthreshold oscillations around a resting state, a bistability that is typical of a subcritical Hopf–Andronov bifurcation (27), for which there is evidence in many interneurons (28) and pyramidal neurons (29, 30). However, only the IS- and ST-type interneurons, with particularly fast K^+ conductances, show a wide enough regime of noise-induced switching between spiking and subthreshold oscillations for this switching behavior to be observed in normal recordings.

To elucidate the basis for this difference, we investigated the level of susceptibility of a Hodgkin–Huxley-type biophysical neuron to bistable switching as a function of the time constant of the K^+ conductance. A region of bistability indicates that multiple dynamical attractors coexist and that the initial conditions determine to which attractor the dynamics will converge. In the present case of a neural model, the two attractors are a limit cycle (continuous spiking) and a fixed point (returning to the resting state). Which attractor the neural dynamics converge to is determined by which basin of attraction the dynamics are started in. To provide these initial conditions, we varied a control parameter—the input current—both in the ascending and the descending direction in a continuous simulation run.

For the Hodgkin–Huxley-type model, this demonstrates a region of bistability whose size varies as a function of the time constant of the K^+ conductance (Fig. 4). For fast time constants the region of bistability as a function of input current is substantial; in the present example is has a width of almost 0.1 μA for $\tau_S = 4.1$ ms (Fig. 4*A*). Bistability occurs where the ascending (gray) and the descending (black) symbols are separated. With increasing time constant of the K_S conductance the region of bistability shrinks (e.g., at $\tau_s = 7.7$ ms it is only 0.07 μA wide; Fig. 4*B*) and almost disappears at even longer time constants (e.g., at

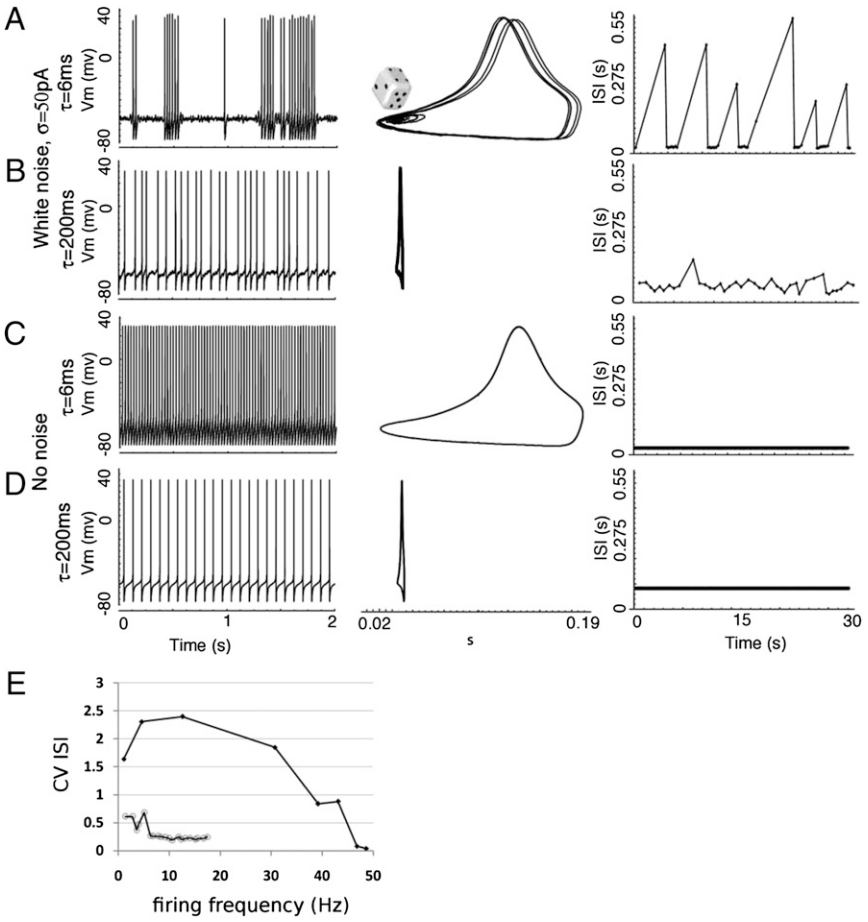

Fig. 3. Reactions to noise in Hodgkin–Huxley-type models of neuronal spiking. Voltage traces (*Left*), phase plane representations of spiking dynamics (*s* vs. V_m, *Center*), and ISIs in response to dc depolarization (*Right*). (*A*) $\tau_s = 6$ ms (ST/IS interneuron), $\sigma_{noise} = 50$ pA. Dice, stochastic decision point. (*B*) $\tau_s = 6$ ms, noise-free simulation. (*C*) $\tau_s = 200$ ms (pyramid), $\sigma_{noise} = 50$ pA. (*D*) $\tau_s = 200$ ms, noise-free simulation. $I_{inj} = 260$ pA in all simulations shown. (*E*) CV_{ISI} as a function of the firing frequency for $\tau_s = 6$ ms (♦), $\tau_s = 200$ ms (○), $\sigma_{noise} = 50$ pA, and I_{inj} varied from 100 to 300 pA in steps of 10 pA. Because the minimum required injected current for the model with $\tau_s = 6$ ms is higher, this model fired over a smaller range between 100–300 pA.

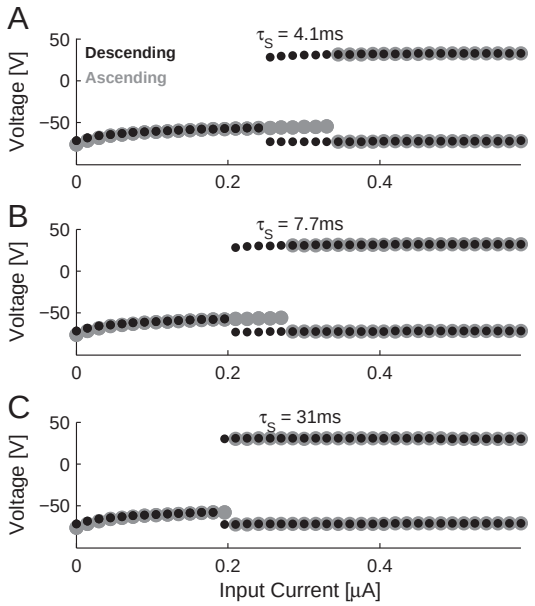

Fig. 4. The time constant of the K_S conductance modifies the bistable region in the Hodgkin–Huxley-type neuron. We estimated a bifurcation diagram by ramping the input current (as the control parameter) in an ascending (gray) and a descending (black) direction for three different values of the time constant of the K_S channel. (*A*) For τ_s = 4.1 ms the model exhibits a wide region of bistability (switching region), indicated by the region where the descending parameter sweep still spikes (two dots indicate the maxima/minima of the spike, whereas one dot indicates the stable fixed point below threshold), whereas the ascending sweep does not yet spike. (*B* and *C*) For larger time constants, the switching region becomes narrower and almost disappears at even higher values (>20 ms).

τ_s = 7.7 ms it is only 0.02 μA wide). The present analysis was applied to the Morris–Lecar model as well (*SI Text* and Fig. S1) with qualitatively similar results.

Based on this bifurcation analysis we confirmed that a significantly wider, bistable region in a spiking system with a Hopf–Andronov bifurcation exists in both a biophysical Hodgkin–Huxley-type and the Morris–Lecar model only for fast, hyperpolarizing K^+ conductances. Because noise-induced switching is possible only in this bistable region, this phenomenon is dependent on fast, interneuronal K^+ conductances. This is also consistent with the observation that intrinsically irregular spike trains in cortical neurons are observed only in interneurons with fast K^+ conductances.

Parameter Exploration. Finally, how robust are these results to varying other parameters in the model? To determine the parameter dependence of intrinsically irregular firing in the original, biophysical, neuron model, we ran two-dimensional parameter sweeps over τ_s/g_s, τ_s/c_m, τ_s/I_{inj}, and τ_s/σ_{noise}. When τ_s was smaller, the CV_{ISI} was higher at all values of g_s. When g_s was largest, the range of τ_s where irregular firing occurred was also largest (Fig. 5*A*). Smaller τ_s caused higher CVs at all values of c_m. The same held true for all values of I_{inj}. The higher the I_{inj}, the smaller τ_s had to be to allow for irregular firing and the higher the maximum possible CV_{ISI}.

To investigate the dependence of intrinsically irregular firing on the properties of the injected noise, we conducted simulations using power-law and Ornstein–Uhlenbeck (OU, autocorrelated) noise in addition to the standard Gaussian white noise (Fig. 5*B*). The exponent of the power-law noise was $k = -0.7$, as deduced from the recorded subthreshold voltage fluctuations by deconvolution with the impulse response of the membrane. The parameters for the OU noise mimicked the synaptic bombardment experienced by cortical neurons in vivo (31). The noise amplitude necessary for obtaining an identical CV_{ISI} was reduced an order of magnitude with power-law noise and reduced another order of magnitude with OU noise. This is consistent with previous studies showing that correlated fluctuations are highly effective in evoking spikes (7, 9, 31). All qualitative observations made with Gaussian white noise were confirmed with power-law and OU noise as well.

In parameter regions where $CV_{ISI} \approx 1$, the interspike intervals were approximately Poisson-distributed, similar to the IS behavior, whereas for CV_{ISI} >1.5, spikes were dominantly clustered, resembling the ST pattern. The discrete changes in spiking behavior between regular firing pyramidal neurons, irregular firing IS interneurons, and highly irregular firing ST neurons can be explained as a continuous change in a single parameter, the K^+ conductance time constant τ_s.

Discussion

The study of cortical spike-train statistics has previously focused almost entirely on pyramidal neurons. Pyramidal neurons and

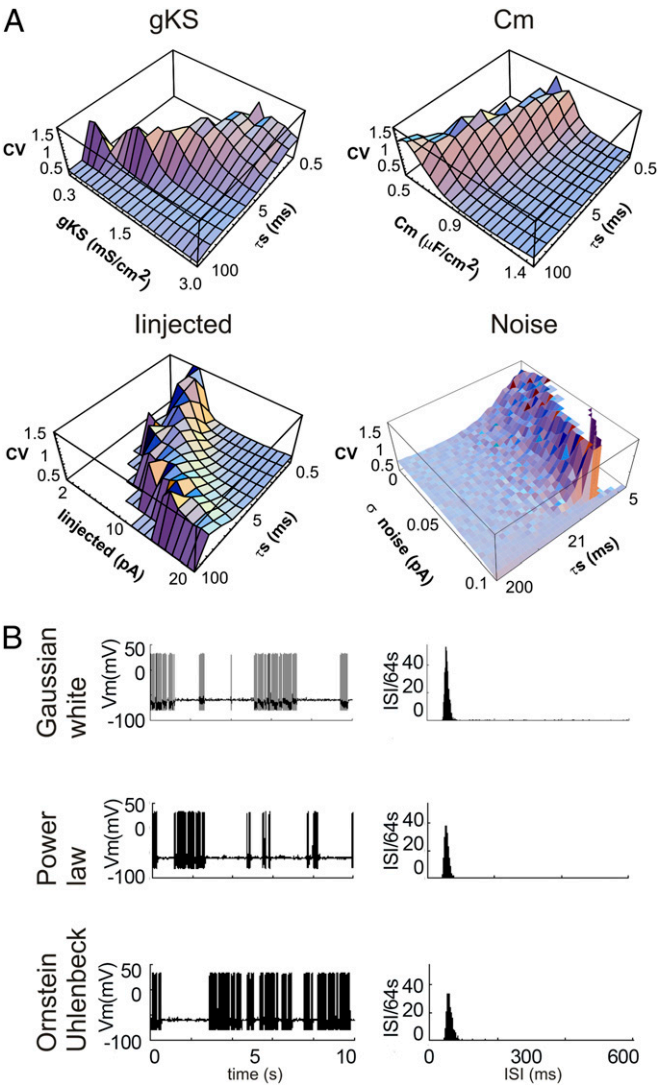

Fig. 5. Dependence of the behavior of the Hodgkin–Huxley-type model on parameter choice and noise type. (*A*) CV_{ISI} as a function of σ_{noise}/τ_s, c_m/τ_s, I_{inj}/τ_s and σ_{noise}/τ_s. (*B*) Spiking behavior (*Left*) and ISI histogram (*Right*) for Gaussian white (*Top*), power-law (λ = 0.7, *Middle*), and Ornstein–Uhlenbeck noise (*Bottom*).

interneurons are markedly different with regard to the location of the axon (32) and the Na^+ currents (32) and K^+ currents (33, 34) involved in spike and AHP generation as well as their input resistance. We have presented recordings and biophysical simulations suggesting that the faster time constant of the K^+ currents could be the decisive difference with respect to spike time variability.

Faster τ_s lead to a more extended bistable region of the Hopf–Andronov bifurcation. In this region, noise-induced switching between spiking and subthreshold oscillating occurs, leading to interneuronal spike trains consisting of bursts, interrupted by nonspiking periods of variable lengths. The mechanism was described in a Hodgkin–Huxley neuron model transitioning to spiking via a Hopf–Andronov bifurcation (24, 25). Here we have demonstrated the importance of a fast K^+ conductance for enabling this mechanism. We further argue that this fast conductance is what causes IS and ST interneurons to spike irregularly, but not other types of interneurons and pyramidal neurons, even if they also spike via a Hopf–Andronov bifurcation.

Interestingly, Badoual et al. (35) achieved high discharge variability in pyramidal neurons by injecting low-pass filtered noise waveform. This represents an approach complementary to ours. Whereas we observed increased discharge irregularity by recording from neurons (IS and ST interneurons) with a fast τ of the K^+ conductances, closer to the time scale of the naturally occurring noise, Badoual et al. changed the time scale of the noise to fit the τ of the slower pyramidal K^+ conductances.

Neural dynamics driven by noise have been reported previously (36).

In a study of the firing of interneurons using a biophysical model of interneurons including g_{Na}, the persistent Na^+ conductance g_{NAp}, g_{KDR}, and g_{Kd}, both the window current and the total g_{Kd} conductance shaped the spiking behavior of the model neurons (37). In this model, a large g_{Kd} and a small window current were necessary for irregular firing. Depending on the exact parameter choice, they reproduced a noise-sensitive delay to firing, as seen in in vitro recordings from some interneurons. They also observe subthreshold oscillations. The switching mechanism described here could also occur in this more complex model (37).

A more intuitive explanation of these dynamics is that with a faster time constant of the K^+ currents, these currents can interact with the noise in a dynamic manner. Only a K^+ current with a fast time constant can react quickly enough to a fast upward/downward fluctuation to move a neuron from/to the stable resting state to/from spiking. When the time constant of the K^+ current is slower, it essentially becomes a constant hyperpolarization at the relevant time scales and does not influence the neuron's fast dynamics anymore.

A neuron "stuck" in the bistable resting state is in a condition where its K^+ current is just too strongly activated and its Na^+ current just too inactivated to allow it to spike. Fast K^+ current dynamics allow switching between this resting state and a spiking regime. Only if its K^+ current is fast enough can this bistable state persist over a range of applied current strengths. If the K^+ currents are too slow, they act more or less like a constant hyperpolarization, and the bistable resting state ceases to exist.

These results raise the question of how a subpopulation of intrinsically irregular interneurons could affect the overall spiking statistics in the cortex. Interneurons interact strongly among themselves and with pyramidal neurons (13, 18). The high sensitivity of interneurons to fluctuations will almost certainly affect the temporal structure of firing in all cortical neurons. Thus, the intrinsically irregular output of ST and IS interneurons may partially account for the irregularity of cortical firing. Additionally, if, as is likely, the fast fluctuations in cortical activity carry information, then ST and IS interneurons will be especially sensitive to this information while their states are in the switching region. This phase-sensitive read-out mechanism would make them ideal candidates for processing information restricted to specific oscillatory phases, as proposed in several coding schemes (38, 39).

Methods

Electrophysiology. Pyramidal neurons and fast-spiking interneurons in layer 2/3 were recorded intracellularly in the slices of mouse visual cortex. All procedures on animals were done in accordance with Salk Institute Institutional Animal Care and Use Committee ethical guidelines. Mice (B6D21/Hsd B6, "black 6," age 28–35 d; Harlan) were anesthetized with halothane and decapitated. The occipital forebrain was removed and glued to a plastic block. Coronal slices of the visual cortex (300 μm) were cut with a Series 1000 vibratome (Pelco) in ice-cold artificial cerebrospinal fluid (ACSF; 125 mM NaCl, 2.5 mM KCl, 1.25 mM NaH_2PO_4, 25 mM NaHCO3, 2 mM $CaCl_2$, 1.3 mM $MgCl_2$, and 10 mM dextrose). Slices were allowed to recover in ACSF at 35 °C for at least 30 min before the start of the recordings.

Recordings were performed under IR-differential interference contrast videomicroscopy in oxygenated ACSF (flow 3 mL/min) at 32 °C. Whole-cell patch-clamp recordings were performed with electrodes ranging from 6 to 8 MΩ. The pipette solution contained 140 mM $KMeSO_4$, 10 mM Hepes, 1.5 mM NaCl, and 0.1 mM EGTA.

The voltage signal was recorded with an Axoclamp-2A amplifier (Axon Instruments), low-pass-filtered at 30 kHz, and digitized at 32 kHz with a PCI-MIO-16E-4 DAQ board (National Instruments). Data acquisition software was custom-written in Lab View 6.1 (National Instruments).

Glutamatergic ionotropic synaptic transmission was blocked with DNQX (6,7-dinitroquinoxaline-2,3-dione) (20 μM) and AP5 [(2R)-amino-5-phosphonopentanoate] (50 μM) and GABAergic ionotropic transmission with bicuculline (10 μM). Action potential firing was evoked by injecting dc current via the patch-electrode and series of 0.5-s pulses and continuous stretches spanning 32–64 s were recorded. Drugs were purchased from Sigma and Fisher.

Simulations. The Hodgkin–Huxley model of the interneuron had one compartment with ion channels, described in *SI Text*.

The Morris–Lecar oscillator model (40) had two state variables, as described in *SI Text*.

We used the ordinary differential equation solvers NEURON (41) and XPP (42). All simulation code is available upon request from K.M.S. or the Yale Model Database (https://senselab.med.yale.edu/modeldb/).

Bifurcation Analysis. We studied the structure of the phase space as a function of a control parameter using bifurcation analysis. For the Morris–Lecar model, we used XPP's AUTO function to plot bifurcation diagrams for different values of the injected current. For the biophysical neuron model, we directly varied the injected current in a continuous simulation run in NEURON. In both cases we then compared the width of the bistable region as a function of the time constant of the K_S conductance. The bistable region is defined as the region where the neural behavior can alternatively be spiking or resting, depending on the initial conditions. For the biophysical model we ramped the current both in an ascending and a descending direction, thus providing a resting or a spiking initial condition, respectively.

ACKNOWLEDGMENTS. We thank Dr. Lee Campbell for providing data acquisition software; Drs. Jean-Marc Fellous, Peter J. Thomas, Paul Tiesinga, Jürgen Jost, Priscilla E. Greenwood, Peter Rowat, and Charles F. Stevens for helpful discussions; and Dr. G. Bard Ermentrout for assistance with XPP. Financial support was provided by the Deutsche Forschungsgemeinschaft (K.M.S.), the Studienstiftung des Deutschen Volkes (B.E.), and the Howard Hughes Medical Institute and the Office of Naval Research N00014-97-1-0422 (T.J.S.).

1. Noda H, Adey WR (1970) Firing variability in cat association cortex during sleep and wakefulness. *Brain Res* 18(3):513–526.
2. Burns BD, Webb AC (1976) The spontaneous activity of neurones in the cat's cerebral cortex. *Proc R Soc Lond B Biol Sci* 194(1115):211–223.
3. Destexhe A, Contreras D, Steriade M (1999) Spatiotemporal analysis of local field potentials and unit discharges in cat cerebral cortex during natural wake and sleep states. *J Neurosci* 19(11):4595–4608.
4. Knierim JJ, van Essen DC (1992) Neuronal responses to static texture patterns in area V1 of the alert macaque monkey. *J Neurophysiol* 67(4):961–980.
5. Softky WR, Koch C (1993) The highly irregular firing of cortical cells is inconsistent with temporal integration of random EPSPs. *J Neurosci* 13(1):334–350.
6. Singer W (1999) Time as coding space? *Curr Opin Neurobiol* 9(2):189–194.
7. Salinas E, Sejnowski TJ (2000) Impact of correlated synaptic input on output firing rate and variability in simple neuronal models. *J Neurosci* 20(16):6193–6209.

8. Fellous J-M, Rudolph M, Destexhe A, Sejnowski TJ (2003) Synaptic background noise controls the input/output characteristics of single cells in an in vitro model of in vivo activity. *Neuroscience* 122(3):811–829.
9. Stevens CF, Zador AM (1998) Input synchrony and the irregular firing of cortical neurons. *Nat Neurosci* 1(3):210–217.
10. Buhl EH, Tamás G, Fisahn A (1998) Cholinergic activation and tonic excitation induce persistent gamma oscillations in mouse somatosensory cortex in vitro. *J Physiol* 513(Pt 1):117–126.
11. Fisahn A, Pike FG, Buhl EH, Paulsen O (1998) Cholinergic induction of network oscillations at 40 Hz in the hippocampus in vitro. *Nature* 394(6689):186–189.
12. Gerstein GL, Mandelbrot B (1964) Random walk models for the spike activity of a single neuron. *Biophys J* 4:41–68.
13. Thomson AM, West DC, Wang Y, Bannister AP (2002) Synaptic connections and small circuits involving excitatory and inhibitory neurons in layers 2-5 of adult rat and cat neocortex: Triple intracellular recordings and biocytin labelling in vitro. *Cereb Cortex* 12(9):936–953.
14. Tamás G, Szabadics J, Lörincz A, Somogyi P (2004) Input and frequency-specific entrainment of postsynaptic firing by IPSPs of perisomatic or dendritic origin. *Eur J Neurosci* 20(10):2681–2690.
15. Larkum ME, Zhu JJ, Sakmann B (1999) A new cellular mechanism for coupling inputs arriving at different cortical layers. *Nature* 398(6725):338–341.
16. Douglas RM, Goddard GV, Riives M (1982) Inhibitory modulation of long-term potentiation: Evidence for a postsynaptic locus of control. *Brain Res* 240(2):259–272.
17. Markram H, et al. (2004) Interneurons of the neocortical inhibitory system. *Nat Rev Neurosci* 5(10):793–807.
18. Gupta A, Wang Y, Markram H (2000) Organizing principles for a diversity of GABAergic interneurons and synapses in the neocortex. *Science* 287(5451):273–278.
19. Kim U, McCormick DA (1998) The functional influence of burst and tonic firing mode on synaptic interactions in the thalamus. *J Neurosci* 18(22):9500–9516.
20. Englitz B, Stiefel KM, Sejnowski TJ (2008) Irregular firing of isolated cortical interneurons in vitro driven by intrinsic stochastic mechanisms. *Neural Comput* 20(1):44–64.
21. Hille B (2001) *Ion Channels of Excitable Membranes* (Sinauer Associates, Sunderland, MA), 3rd Ed.
22. Coetzee WA, et al. (1999) Molecular diversity of K^+ channels. *Ann N Y Acad Sci* 868: 233–285.
23. Stiefel KM, Fellous JM, Thomas PJ, Sejnowski TJ (2010) Intrinsic subthreshold oscillations extend the influence of inhibitory synaptic inputs on cortical pyramidal neurons. *Eur J Neurosci* 31(6):1019–1026.
24. Rowat PF, Greenwood PE (2011) Identification and continuity of the distributions of burst-length and interspike intervals in the stochastic Morris-Lecar neuron. *Neural Comput* 23(12):3094–3124.
25. Rowat P (2007) Interspike interval statistics in the stochastic Hodgkin-Huxley model: Coexistence of gamma frequency bursts and highly irregular firing. *Neural Comput* 19(5):1215–1250.
26. Ermentrout GB, Terman TH (2010) *Mathematical Foundations of Neuroscience* (Springer, Berlin).
27. Izhikevich EM (2010) *Dynamical Systems in Neuroscience: The Geometry of Excitability and Bursting* (MIT Press, Cambridge, MA).
28. Tateno T, Robinson HPC (2007) Phase resetting curves and oscillatory stability in interneurons of rat somatosensory cortex. *Biophys J* 92(2):683–695.
29. Tsubo Y, Takada M, Reyes AD, Fukai T (2007) Layer and frequency dependencies of phase response properties of pyramidal neurons in rat motor cortex. *Eur J Neurosci* 25(11):3429–3441.
30. Stiefel KM, Gutkin BS, Sejnowski TJ (2008) Cholinergic neuromodulation changes phase response curve shape and type in cortical pyramidal neurons. *PLoS ONE* 3(12): e3947.
31. Destexhe A, Rudolph M, Fellous J-M, Sejnowski TJ (2001) Fluctuating synaptic conductances recreate in vivo-like activity in neocortical neurons. *Neuroscience* 107(1): 13–24.
32. Martina M, Vida I, Jonas P (2000) Distal initiation and active propagation of action potentials in interneuron dendrites. *Science* 287(5451):295–300.
33. Martina M, Schultz JH, Ehmke H, Monyer H, Jonas P (1998) Functional and molecular differences between voltage-gated K^+ channels of fast-spiking interneurons and pyramidal neurons of rat hippocampus. *J Neurosci* 18(20):8111–8125.
34. Lien CC, Martina M, Schultz JH, Ehmke H, Jonas P (2002) Gating, modulation and subunit composition of voltage-gated K(+) channels in dendritic inhibitory interneurones of rat hippocampus. *J Physiol* 538(Pt 2):405–419.
35. Badoual M, Rudolph M, Piwkowska Z, Destexhe A, Bal T (2005) High discharge variability in neurons driven by current noise. *Neurocomputing* 65–66:493–498.
36. Longtin A, Hinzer K (1996) Encoding with bursting, subthreshold oscillations, and noise in mammalian cold receptors. *Neural Comput* 8(2):215–255.
37. Golomb D, et al. (2007) Mechanisms of firing patterns in fast-spiking cortical interneurons. *PLOS Comput Biol* 3(8):e156.
38. O'Keefe J, Recce ML (1993) Phase relationship between hippocampal place units and the EEG theta rhythm. *Hippocampus* 3(3):317–330.
39. Vinck M, et al. (2010) Gamma-phase shifting in awake monkey visual cortex. *J Neurosci* 30(4):1250–1257.
40. Rinzel J, Ermentrout GB (1989) *Methods in Neuronal Modeling*, eds Koch C, Segev I (MIT Press, Cambridge, MA), pp 135–169.
41. Carnevale NT, Hines ML (2009) *The NEURON Book* (Cambridge Univ Press, Cambridge, UK), 1st Ed.
42. Ermentrout B (2002) *Simulating, Analyzing, and Animating Dynamical Systems: A Guide to Xppaut for Researchers and Students (Software, Environments, Tools)* (Society for Industrial and Applied Mathematics, Philadelphia, PA), 1st Ed.

Supporting Information

Stiefel et al. 10.1073/pnas.1305219110

SI Text

Biophysical Neuron Model. In NEURON, we implemented a single-compartmental model of a spiking neuron described by modified Hodgkin–Huxley equations (1). We added one K^+ conductance, g_{KS}, mediating the afterhyperpolarization (AHP) to the original formalism. The equations are

$$c_m dV/dt = g_l(E_K - V) + m^3 h\, g_{Na}(E_{Na} - V) + n^4\, g_{KDR}(E_K - V) + s\, g_{KS}(E_K - V) + I_{app} + I_{noise},$$

where V is the voltage, m and h are the activation and inactivation states of the fast Na^+ conductance, and n and s are the activation variables for the delayed-rectifier and AHP K^+ conductances. Their time evolution is governed by

$$\tau_m dm/dt = m_{inf} - m$$

$$\tau_m = 1/(\alpha + \beta)$$

$$m_{inf} = \alpha/(\alpha + \beta)$$

with equivalent equations for h, m, and s. The expressions for α and β of m are

$$\alpha = 0.091(V + 38)/(1 - \exp(-(V + 38)/5)$$

$$\beta = -0.062(V + 38)/(1 - \exp((V + 38)/5).$$

The expressions for α and β of h are

$$\alpha = 0.016\ \exp((-55 - V)/15))$$

$$\beta = 2.07/\exp((17 - V)/21) + 1).$$

The expressions for α and β of n are

$$\alpha = 0.044(V + 53)/(1 - \exp(-0.22(V + 53)))$$

$$\beta = 0.75\ \exp(0.025(V + 50)).$$

The expressions governing s are

$$\tau_s = 6 \text{ to } 200 \text{ ms, depending on the simulation.}$$

$$s_{inf} = 1\Big/\left(1 + e^{0.2(-53.4\ -\ V)}\right)$$

The maximum conductances were $g_l = 2 \times 10^{-5}$ S·cm^{-2}, $g_{Na} = 0.12$ S·cm^{-2}, $g_{KDR} = 0.1$ S·cm^{-2}, $g_{KS} = 0.003$ S·cm^{-2}, and the reversal potentials $E_{Na} = 50$ mV and $E_K = -76$ mV. Membrane capacitance was $c_m = 0.6$ μF·cm^{-2}. The injected current noise, I_{noise}, was drawn from a Gaussian white distribution.

The parameters of the model were chosen to reproduce the firing of cortical neurons. As outlined above, we varied the time constant of K_S, τ_s, between 6 and 200 ms to reproduce the fast and slow AHPs of interneurons and pyramidal neurons, respectively. Numerical integration was performed with a Crank–Nicolson exponential algorithm, with a 0.025-ms time step.

Morris–Lecar Model. To explore the bifurcations leading to spiking, we investigated a variant of the Morris–Lecar oscillator model (2). This model is a simple oscillator with two state variables, and although it shares many qualitative features with more complex and biophysically realistic model neurons, it is more amenable to thorough mathematical analysis.

The equations governing the modified Morris–Lecar model are as follow:

$$dV/dt = \left(I_{app} + W g_w + g_l(E_l - V) + g_k w(E_K - V) - I_{Ca}\right)$$

$$dw/dt = \left(l_{amn}(V)\left(n_{inf}(V) - w\right)\right)/\tau_s$$

$$m_{inf}(V) = 0.5(1 + \tanh((V - V_1)/V_2))$$

$$n_{inf}(V) = 0.5(1 + \tanh((V - V_3)/V_4))$$

$$l_{amn}(V) = \phi \cosh((V - V_3)/(2V_4))$$

$$I_{Ca} = g_{Ca} m_{inf}(V)(V - 1),$$

with the parameter values $\phi = 0.333$, $V_1 = -0.01$, $V_2 = 0.15$, $V_3 = 0.1$, $V_4 = 0.145$, $g_{Ca} = 1.33$, $E_K = -0.7$, $V_1 = -0.5$, $g_K = 3$, $g_l = 0.5$, $\tau_s = 0.5$–10, and $g_w = 0$–0.05 and where V and w are the state variables for the voltage and the K^+ current activation, respectively, and W is a Wiener process (a noise source). The Ca^{2+} current is treated as instantaneous. Our modifications of the classic Morris–Lecar model are the introduction of a time constant for the K^+ current, τ_w, the introduction of the Wiener process, and the increase of the Ca^{2+} conductance, g_K, from 2 to 3.

Numerical integration was performed with a fourth-order Runge–Kutta algorithm, with a 0.025-ms time step.

Bifurcation Analysis. We further investigated the origin of the different spiking properties by introducing the same potassium channel into the Morris–Lecar model (2) with different K_S time constants. The Morris–Lecar oscillator was originally designed as a model of the barnacle giant muscle fiber but has since served as a useful generic model for neural oscillations (3, 4). Because it is only two-dimensional and simpler than the more complex, biophysical, more realistic neuron models, it is also more amendable to more mathematical analysis. For example, it is possible to analyze a bifurcation diagram of the Morris–Lecar model, revealing the steady-state behavior of a system (rest or spiking) as a control parameter (injected current) is varied. Essentially, each plane perpendicular to the bifurcation diagram is a phase plane with a steady-state trajectory; only the maxima and minima of an oscillation are plotted.

The bifurcation diagram of the Morris–Lecar oscillator with a fast K_S conductance time constant had a Hopf–Andronov bifurcation, with a bistable region ranging from $I_{app} = 0.3084$–0.3634, a range of 0.550 (Fig. S1, *Top*). When we slowed down the K_S conductance time constant τ_s to 2 ms, the extent of the bistable region as a function of I_{app} was reduced to a range of 0.416 (Fig. S1, *Middle*). With $\tau_s = 10$, the bistable region all but disappeared, with an I_{app} range of 0.081 (Fig. S1, *Bottom*). The loss of the bistable region in the Morris–Lecar model also went hand in hand with the loss of irregular spiking and subthreshold oscillations. Setting I_{app} to a value 0.01 above the Hopf bifurcation point, the firing was irregular and interrupted by episodes of subthreshold oscillations with fast time constants, but became regular and uninterrupted with $\tau_s = 10$.

1. McCormick DA, Huguenard JR (1992) A model of the electrophysiological properties of thalamocortical relay neurons. *J Neurophysiol* 68(4):1384–1400.
2. Rinzel J, Ermentrout GB (1989) *Methods in Neuronal Modeling*, eds Koch C, Segev I (MIT Press, Cambridge, MA), pp 135–169.
3. Gutkin BS, Ermentrout GB (1998) Dynamics of membrane excitability determine interspike interval variability: A link between spike generation mechanisms and cortical spike train statistics. *Neural Comput* 10(5):1047–1065.
4. Prescott SA, Ratté S, De Koninck Y, Sejnowski TJ (2006) Nonlinear interaction between shunting and adaptation controls a switch between integration and coincidence detection in pyramidal neurons. *J Neurosci* 26(36):9084–9097.

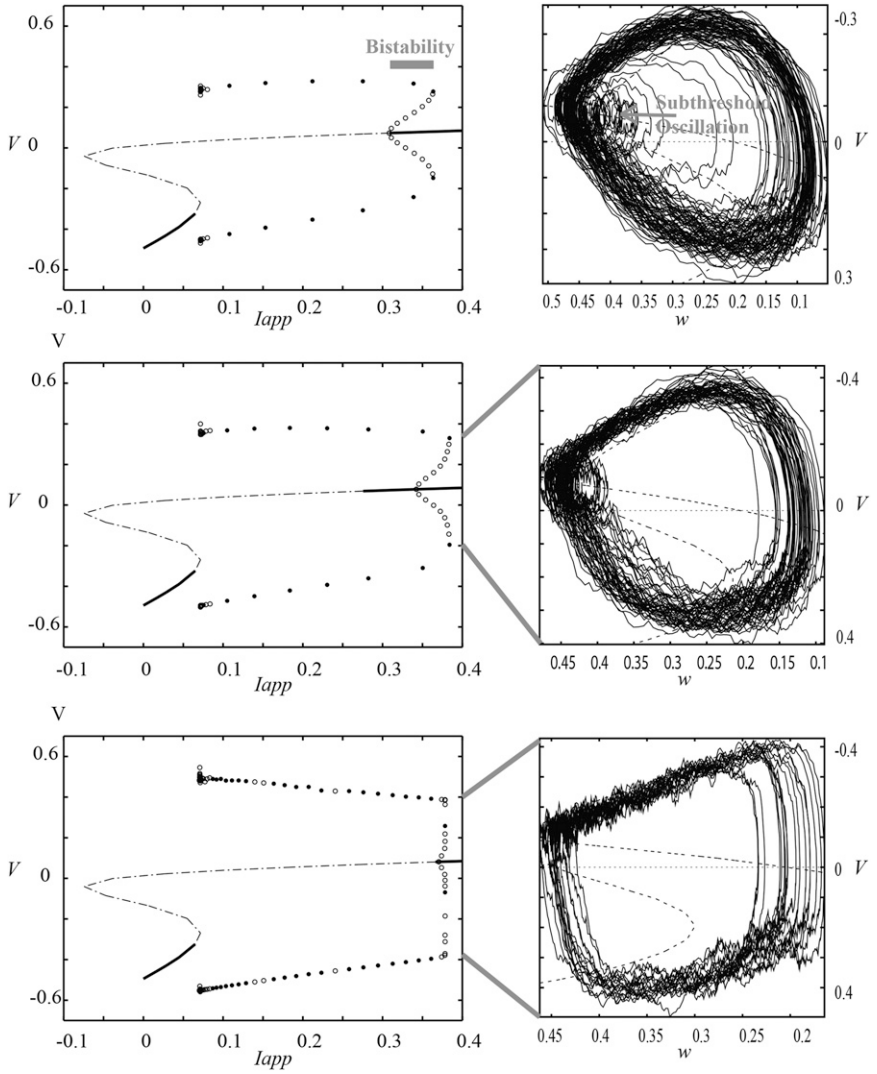

Fig. S1. The K_S conductance time constant changes the width of the bistable region in the Morris–Lecar model neuron. Bifurcation diagrams (*Left*) and trajectories in the phase plane of a Morris–Lecar model with a K_S time constant of $\tau_s = 1$ (*Top*), $\tau_s = 2$ (*Middle*), and $\tau_s = 10$ (*Bottom*). Note the decreasing bistable region and the disappearance of the noise-induced subthreshold oscillations with successively longer τ_s.